

Imaging Patients with Metastatic Castration-Resistant Prostate Cancer Using ^{89}Zr -DFO-MSTP2109A Anti-STEAP1 Antibody

Jorge A. Carrasquillo^{1–3}, Bernard M. Fine⁴, Neeta Pandit-Taskar^{1–3}, Steven M. Larson^{1–3}, Stephen E. Fleming¹, Josef J. Fox¹, Sarah M. Cheal¹, Joseph A. O'Donoghue⁵, Shutian Ruan¹, Govind Ragupathi⁶, Serge K. Lyashchenko⁷, John L. Humm⁵, Howard I. Scher^{6,8}, Mithat Gönen⁹, Simon P. Williams⁴, Daniel C. Danila^{*6,8}, and Michael J. Morris^{*6,8}

¹Department of Radiology, Memorial Sloan Kettering Cancer Center, New York, New York; ²Department of Radiology, Weill Cornell Medical Center, New York, New York; ³Center for Targeted Radioimmunotherapy and Diagnosis, Ludwig Center for Cancer Immunotherapy, New York, New York; ⁴Genentech, South San Francisco, California; ⁵Department of Medical Physics, Memorial Sloan Kettering Cancer Center, New York, New York; ⁶Department of Medicine, Memorial Sloan Kettering Cancer Center, New York, New York; ⁷Radiochemistry and Molecular Imaging Probes Core, Memorial Sloan Kettering Cancer Center, New York, New York; ⁸Joan and Sanford I. Weill Department of Medicine, Weill Cornell Medicine, New York, New York; and ⁹Biostatistics Service, Department of Epidemiology and Biostatistics, Memorial Sloan Kettering Cancer Center, New York, New York

Six-transmembrane epithelial antigen of prostate-1 (STEAP1) is a relatively newly identified target in prostate cancer. We evaluated the ability of PET/CT with ^{89}Zr -DFO-MSTP2109A, an antibody that recognizes STEAP1, to detect lesions in patients with metastatic castration-resistant prostate cancer (mCRPC). **Methods:** Nineteen mCRPC patients were prospectively imaged using approximately 185 MBq/10 mg of ^{89}Zr -DFO-MSTP2109A. ^{89}Zr -DFO-MSTP2109A PET/CT images obtained 4–7 d after injection were compared with bone and CT scans. Uptake in lesions was measured. Fifteen patients were treated with an antibody–drug conjugate (ADC) based on MSTP2109A; ADC treatment–related data were correlated with tumor uptake by PET imaging. Bone or soft-tissue biopsy samples were evaluated. **Results:** No significant toxicity occurred. Excellent uptake was observed in bone and soft-tissue disease. Median SUV_{max} was 20.6 in bone and 16.8 in soft tissue. Sixteen of 17 lesions biopsied were positive on ^{89}Zr -DFO-MSTP2109A, and all sites were histologically positive (1 on repeat biopsy). Bayesian analysis resulted in a best estimate of 86% of histologically positive lesions being true-positive on imaging (95% confidence interval, 75%–100%). There was no correlation between SUV_{max} tumor uptake and STEAP1 immunohistochemistry, survival after ADC treatment, number of ADC treatment cycles, or change in prostate-specific antigen level. **Conclusion:** ^{89}Zr -DFO-MSTP2109A is well tolerated and shows localization in mCRPC sites in bone and soft tissue. Given the high SUV in tumor and localization of a large number of lesions, this reagent warrants further exploration as a companion diagnostic in patients undergoing STEAP1-directed therapy.

Key Words: STEAP1; ^{89}Zr ; antibody; positron; prostate cancer

J Nucl Med 2019; 60:1517–1523

DOI: 10.2967/jnumed.118.222844

Received Nov. 6, 2018; revision accepted Mar. 4, 2019.
For correspondence contact: Jorge A. Carrasquillo, Memorial Sloan Kettering Cancer Center, 1275 York Ave., New York, NY 10065.
E-mail: carrasj1@mskcc.org
*Contributed equally to this work.
Published online May 3, 2019.
COPYRIGHT © 2019 by the Society of Nuclear Medicine and Molecular Imaging.

Prostate cancer–selective antigens have been identified as targets for imaging or therapeutic intervention, including prostate-specific membrane antigen (PSMA) (1–7) and prostate stem cell antigen (PSCA) (8). Six-transmembrane epithelial antigen of prostate (STEAP) comprises a family of 4 novel cell surface markers that are highly expressed in prostate cancer but also present in other cancers and have little cross-reactivity to other normal tissues (9–11). STEAP1 is a novel 339–amino acid cell surface marker. Its exact function has yet to be determined, but it appears to be an ion channel or transporter protein with a role in cell adhesion and may be related to tumor proliferation and invasiveness (9). A role in intracellular communication and tumor growth inhibition in vivo has been shown, as well as a possible role in iron metabolism (11). Previous reports suggest that STEAP1 expression may be a biomarker for worse prognosis of prostate cancer (12).

Because of high expression in prostate and other cancers, STEAP1 has been identified as a promising candidate for therapeutic intervention using antibody–drug conjugates (ADCs), monoclonal antibodies, DNA vaccines, and small noncoding RNAs (13). Preclinical studies with ^{111}In or ^{89}Zr -MSTP2109A anti-STEAP1, an internalizing antibody, showed a correlation between the expression of STEAP1, radiolabeled antibody tumor uptake, and ADC efficacy. However, in 1 cell line, high target expression identified by imaging and immunohistochemistry showed weak efficacy (14). That report suggested that radioimmunotherapy may be used to inform the efficacy of ADC in patients considered for treatment and led to a phase I trial with DSTP3086S, a monomethyl auristatin E (MMAE) conjugated to MSTP2109A anti-STEAP1 antibody (ClinicalTrials.gov identifier NCT01283373) based on the same MSTP2109A antibody described in this report. In addition, ^{89}Zr -DFO-MSTP2109A has detected changes in STEAP1 induced by antiandrogen therapy (15).

In this report, we evaluated the ability of ^{89}Zr -DFO-MSTP2109A to image STEAP1 in patients with metastatic castration-resistant prostate cancer (mCRPC). A separate report will describe the pharmacokinetics, detailed biodistribution, and dosimetry of ^{89}Zr -DFO-MSTP2109A in the initial 6 patients enrolled (16).

MATERIALS AND METHODS

Patient Eligibility and Protocol Design

This was a prospective single-center phase I/II imaging study using ^{89}Zr -positron-labeled DFO-MSTP2109A, an anti-STEAP1 antibody, in 19 patients with mCRPC. Our institutional review board approved the study, and all patients gave written informed consent (ClinicalTrials.gov identifier NCT01774071). All patients were required to have histologically confirmed progressing mCRPC with documented metastatic disease on bone scans, CT, or MRI according to the Prostate Cancer Working Group 2 criteria. The patients had a Karnofsky score of more than 60%, a platelet count of at least $75,000/\mu\text{L}$, an absolute neutrophil count of at least $1,000/\mu\text{L}$, a bilirubin level of less than 1.5 times the upper limit of normal, an alanine aminotransferase/aspartate aminotransferase level of less than 2.5 times the upper limit of normal, and an estimated glomerular filtration rate of more than $30\text{ mL/min}/1.73\text{ m}^2$. All patients had an immunohistochemistry determination of a STEAP1 antigen presence of 1+ or above on tumor tissue (Ventana Medical Systems); in addition, most patients had undergone research biopsy just before ^{89}Zr -DFO-MSTP2109A imaging or shortly afterward as part of another research protocol or as clinically indicated.

A parallel therapeutic phase I trial with DSTP3086S ADC based on monomethyl auristatin conjugated to MSTP2109A (ClinicalTrials.gov identifier NCT01283373) was also accruing at our institution (17). Fifteen of our patients were subsequently enrolled into the DSTP3086S trial, with the other 4 no longer meeting the entry criteria for the ADC trial. The ADC trial is not the subject of this report and will be reported elsewhere.

Antibody Characteristics

MSTP2109A is a humanized IgG1 monoclonal antibody that binds to STEAP1. It was produced under good-manufacturing-practice conditions by Genentech and was conjugated with desferrioxamine (DFO) under good-manufacturing-practice conditions by the Memorial Sloan Kettering Clinical Grade Production Core Facility (18). The antibody was radiolabeled with ^{89}Zr (a positron emitter with a 78.4-h radioactive half-life) by Memorial Sloan Kettering's Radiochemistry and Molecular Imaging Probe Core Facility using methods previously described (19), in compliance with the chemistry, manufacturing, and controls requirements for a Food and Drug Administration-approved investigational new drug (approval 116,724).

Imaging and Whole-Body Analysis

All patients underwent delayed imaging at a median of 6 d after injection (range, 4–7 d). This imaging time was based on a serial biodistribution and pharmacokinetic evaluation conducted on the first 6 patients (data not shown), who received the same antibody activity and mass as the subsequent patients. Imaging was performed on a GE Healthcare Discovery STE PET/CT scanner in 3-dimensional mode using iterative reconstruction with attenuation, scatter, and other standard corrections applied as for clinical ^{18}F -FDG imaging. Images were obtained from the top of the skull to the proximal thigh using a median of 7 min per field of view.

^{89}Zr -DFO-MSTP2109A images were read independently by 3 experienced nuclear medicine physicians, 2 of whom were completely masked to any data or imaging and a third who had previously reviewed the patient history, because he was the principal investigator of the trial, but had not reviewed any images. A standardized form for bone and soft-tissue lesion sites, including organs and nodes, was used for reading the 3 different scans (^{89}Zr -DFO-MSTP2109A, CT and bone scan). Liver and lung sites were assigned to right and left sides, and major lymph node regions were designated separately to neck, chest, abdomen, and pelvic regions. Images read as definitely positive or probably positive were considered positive; those read as unsure, probably negative, or definitely negative were considered negative.

Sites deemed positive by at least 2 of the 3 readers were considered positive.

Localization in tumor was defined as focal accumulation greater than adjacent or contralateral background in areas where physiologic activity was not expected. All images were reviewed on a dedicated PET analysis workstation (AWS [GE Healthcare] or Hybrid viewer [Hermes Medical Solutions]). Volumes of interest were placed visually over bone or soft-tissue tumors and the atrial blood pool. SUV_{max} or SUV_{mean} normalized to body weight [(kBq/mL activity in region)/(kBq injected activity/body weight in g)] was obtained using Hermes software. For correlation to immunohistochemistry, we also determined SUV_{peak} in addition to SUV_{max} in the site of fresh lesion biopsies. Separate readers, masked to all other studies, identified positive sites of tumor uptake using the above-described scale in bone scans or CT.

Evaluation for Toxicity

Patients' vital signs were monitored at baseline before injection and every 30 min for 2 h after injection and at the 4- to 7-d imaging time. Adverse events were documented using version 4 of the Common Terminology Criteria for Adverse Events. Safety was assessed from the period of informed consent to 1 wk after administration of ^{89}Zr -DFO-MSTP2109A.

Statistics

Descriptive statistics included median or mean, SD, and correlation. Groups were compared using the paired t test and the Pearson or Spearman correlation coefficient using SigmaStat, version 3.5 (Systat Software Inc.). Because no gold standard was available, a known site of disease was defined as any lesion identified by bone scanning or CT (bone or soft tissue); furthermore, any bone lesion seen on CT or bone scanning was considered positive for conventional imaging modalities.

The presence of many lesions, of which only a small number can be biopsied, presents a challenge for imaging studies of multifocal metastatic cancer and precludes the use of traditional metrics of diagnostic accuracy such as sensitivity, specificity, and predictive value. To partially remedy this problem, we have used a Bayesian approach to apply information gleaned from biopsied lesions to project the number of cancerous lesions among the unbiopsied ones as described in the appendix of Pandit-Taskar et al. (20). This approach uses the Bayes theorem to calculate the conditional expectation of the number of cancerous lesions among unbiopsied sites given the proportion of cancerous lesions among biopsied sites. To formalize this line of thinking, we denote by θ the probability that an imaged lesion is cancerous. Before observing the biopsy data, we have no information on θ other than the fact that it must be between 0 and 1. We represent this by a uniform distribution, also known as a β -distribution with shape and scale parameters equal to 1:

$$P(\theta) \sim \beta(1, 1).$$

If there are n sites biopsied and x of them are histology- and PET-positive, the likelihood function can be written as

$$P(x) \sim \text{Bin}(n, x)$$

and the posterior distribution of θ is now

$$P(\theta|x) \sim \text{Beta}(x + 1, n - x + 1).$$

This distribution is used to derive an estimate for θ (posterior mean) as well as a confidence interval (highest posterior density region). The marginal distribution of θ can then be used to predict the expected number of positive lesions among unbiopsied lesions. This requires the assumption that the prevalence of positive lesions is similar among biopsied and unbiopsied lesions.

RESULTS

Radiolabeling

The mean radiosynthesis yield was 81% ($n = 19$; range, 64%–92%). The product radiochemical purity was 99.8% (range, 98.7%–100%), as measured by radio–thin-layer chromatography. The median specific activity of the radiolabeled product was 88 MBq/mg (range, 67–1,283 MBq/mg). The median immunoreactivity fraction was 96% (range, 91%–99%), as determined by a Lindmo type assay, using 293/STEAP1c.LB50 cells supplied by Genentech, Inc. Patients received a median injection of 185 MBq (range, 170–199 MBq) containing a median mass of 2.39 mg (range, 1.87–2.92 mg) of the radiolabeled ^{89}Zr -DFO-MSTP2109A, which was supplemented with the nonradiolabeled carrier DFO-MSTP2109A for a total antibody administered mass of 10 mg. In accordance with the criteria in our protocol, we did not evaluate a higher mass of antibody given that the median volume of distribution was close to plasma volume and the lowest β half-life in plasma was long (105 h, suggesting there was not a large normal antigen sink), and furthermore, high-contrast imaging was obtained with the 10-mg mass.

Patients

A total of 20 patients provided written informed consent, but 1 patient declined to participate. Thus, 19 consecutive patients were analyzed, with a median age of 65 y (range, 47–79 y). Of these patients, 6 underwent serial imaging and blood draws. Pharmacokinetics, time course of imaging, and dosimetry data will be reported separately (16). Nonetheless, a representative time course of uptake is shown in Supplemental Figure 1, which also describes the normal biodistribution (supplemental materials are available at <http://jnm.snmjournals.org>). The blood pool in early images decreased considerably over time, particularly in patients with extensive bone involvement (Fig. 1).

Immunohistochemistry grading for STEAP1 on fresh or archival tissue showed 3+ ($n = 6$), 2+ ($n = 9$), and 1+ ($n = 4$). All patients had a baseline prostate-specific antigen (PSA) determination within 2 wk before antibody injection and a median PSA of 30.5 ng/mL (range, 1.0–1,806 ng/mL). All patients had a median of 4 (range, 2–8) prior prostate-directed therapeutic regimens. Fifteen patients subsequently participated in a separate protocol using escalating doses of DSTP3086S ADC (MSTP2109 antibody-based drug conjugate) and received 1–21 cycles of treatment with the ADC (median, 5). Six of these patients discontinued the ADC because of adverse events. Only 9 patients remained on the drug until progression, thus limiting assessment because of the small number of patients evaluable for response.

Patient-Based Analysis

The distribution of bone lesions per patient is shown in Table 1. All patients were considered positive for bone lesions on ^{89}Zr -DFO-MSTP2109A, although 1 (patient 17) had a single bone lesion on ^{89}Zr -DFO-MSTP2109A. Eight patients were considered to have soft-tissue disease on ^{89}Zr -DFO-MSTP2109A, compared with 6 of 19 on CT (Table 1). Representative scans are shown in Figure 1, and the distribution of soft-tissue lesions is shown in Table 1.

Lesion-Based Analysis

Localization of ^{89}Zr -DFO-MSTP2109A in suspected bone metastases was observed in all patients (Table 1). In total, 515 sites were positive on ^{89}Zr -DFO-MSTP2109A.

Four patients underwent 5 biopsies of soft-tissue sites positive on ^{89}Zr -DFO-MSTP2109A, each with confirmation of tumor involvement in the biopsied sites. In 3 of these patients (patients 13, 14, and 17), 3

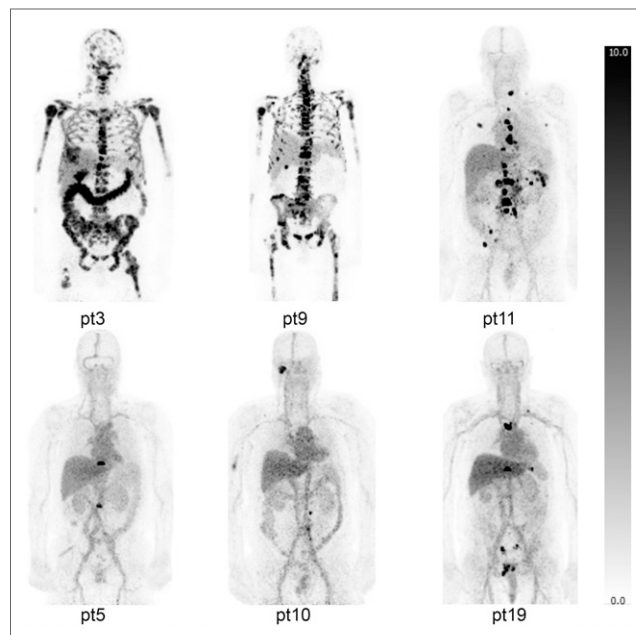


FIGURE 1. ^{89}Zr -DFO-MSTP2109A maximum-intensity projections of selected patients with bone metastases of various extents. Images were acquired at 6 d after injection and are displayed at same gray scale with SUV_{max} of 10. Patients in upper panel (particularly patients 3 and 9) have extensive metastatic bone disease. Uptake in noninvolved bone is low and not definitely seen in projection images. Physiologic blood-pool activity was prominent soon after injection, and much less blood-pool activity is seen in late images in those with more extensive bony disease. Uptake in liver is partially reflective of blood-pool activity and parenchymal accumulation. Low-level uptake is also noted in kidneys, and variable uptake is noted in bowel (intraluminal), which probably represents route of excretion.

biopsied tumors were identified only on ^{89}Zr -DFO-MSTP2109A (Supplemental Table 1). An example of soft-tissue uptake is shown in Figure 2.

Quantitative Analysis

Analysis of the bone lesions ($n = 18$ patients) with the highest ^{89}Zr -DFO-MSTP2109A uptake showed a median SUV_{max} of 20.6 (range, 4.4–59.3; Supplemental Table 1). Patient 4 had a low SUV_{max} of 4.4 in the hottest bone lesion; this patient was atypical, with poorly differentiated prostate cancer at 47 y old. Analysis of the highest SUV_{max} in any soft-tissue lesion per patient ($n = 9$) showed a median SUV_{max} of 16.8 (range, 9.0–24.0; Supplemental Table 1).

The extent of bone involvement on ^{89}Zr -DFO-MSTP2109A varied and was easily visualized. Patients with the most extensive bone disease had faster blood clearance of the antibody (Figs. 1 and 3). A significant negative correlation between the number of bone lesions identified and the amount of activity in the blood (SUV_{mean}) was evident on the last day of imaging, which ranged from 4 to 7 d (Pearson $r = -0.78$; $P < 0.0001$; $n = 19$). When only patients whose last scan was at 6 d ($n = 16$) were analyzed, the correlation was even more marked (Pearson $r = -0.91$; $P < 0.0001$) (Fig. 3).

Various correlations were performed to determine whether tumor uptake was related to immunohistochemistry levels, PSA levels (possible index of tumor burden), or indices of tumor response in patients undergoing DSTP3086S ADC (Supplemental Table 2). SUV_{max} in tumor did not correlate with time from injection to time of death, time on study drug, number of DSTP3086S ADC treatment injections, baseline PSA level, nadir PSA while on treatment with DSTP3086S ADC, or immunohistochemistry level (Table 2).

TABLE 1
Positive Findings by Imaging Modality

Patient no.	Bone lesions				Soft-tissue lesions*	
	⁸⁹ Zr-DFO-MSTP2109A+	Bone scan+	CT+	CIM+	⁸⁹ Zr-DFO-MSTP2109A+	CT+
1	34	31	16	32	1	1
2	71	73	7	73	0	0
3	80	88	74	88	6	2
4	8	54	50	66	0	0
5	3	4	5	8	0	0
6	32	41	17	45	0	0
7	27	30	22	31	0	0
8	40	84	71	85	0	0
9	83	80	31	80	5	1
10	4	2	0	2	2	2
11	17	14	7	14	8	3
12	8	30	10	33	0	0
13	9	22	17	25	4	0
14	5	6	13	14	6	0
15	30	38	37	51	0	0
16	20	11	4	11	0	0
17	1	0	0	0	6	2
18	32	27	14	31	0	0
19	11	15	18	19	0	0
Total	515	650	413	708	38	11

*Nodes, liver, lung, and prostatic bed.

Because of potential differences between SUV_{max} and SUV_{peak} , we also correlated uptake in the 6 fresh biopsied lesions with their immunohistochemistry status (Table 2).

Biopsy Data

Because ethically or practically one cannot biopsy all suggestive ⁸⁹Zr-DFO-MSTP2109A sites, we relied on biopsies performed

under other research protocols or for clinical indications either before ($n = 5$) or after ($n = 12$) ⁸⁹Zr-DFO-MSTP2109A imaging. Fifteen of 19 patients had 17 relatively contemporaneous biopsies (i.e., performed from 35 d before 71 d after injection of ⁸⁹Zr-DFO-MSTP2109A), showing ⁸⁹Zr-DFO-MSTP2109A uptake in 11 of 12 bone sites biopsied and all 5 soft-tissue sites; all of these were performed before any ADC treatment (Supplemental Table 1). Pathologic examination showed that all biopsied sites were

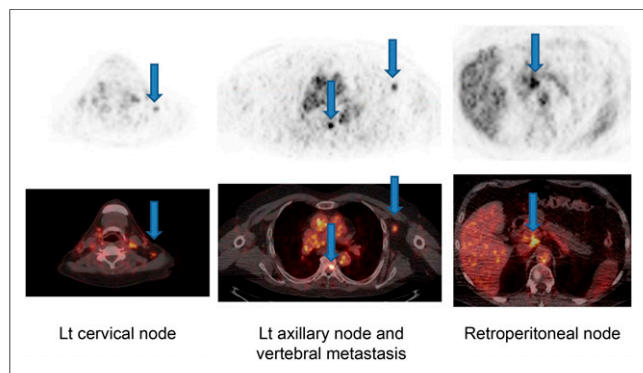


FIGURE 2. ⁸⁹Zr-DFO-MSTP2109A images of patient 13 obtained 6 d after injection. Images showed bone uptake in vertebral lesion (middle panel, midline arrow), in addition to uptake in left axillary node (middle panel arrow in left axilla) that was biopsy-proven metastatic disease. Left cervical nodal uptake (left panel, arrow) and retroperitoneal node (right panel, arrow) showed abnormal uptake. Although these were negative on concurrent CT, follow-up ¹⁸F-FDG scan showed mild uptake at these sites.

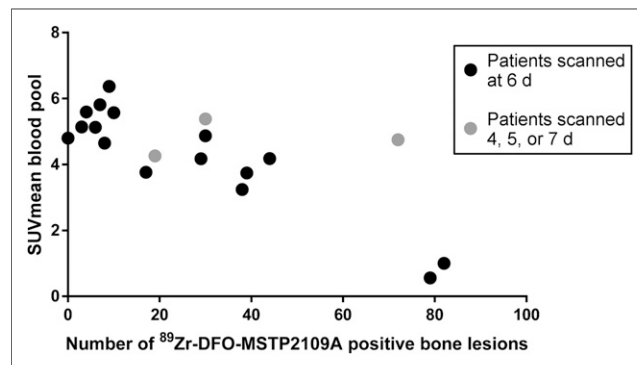


FIGURE 3. Number of lesions identified on ⁸⁹Zr-DFO-MSTP2109A correlated negatively with clearance of radioactivity from blood pool. SUV_{mean} in blood was lower in patients with higher number of lesions when all 19 patients were considered (last scan, 4–8 d) (Pearson $r = -0.78$, $P = 0.0001$) or when patients were scanned on most common day, which was 6 d ($n = 16$) (Pearson $r = -0.91$, $P < 0.0001$).

TABLE 2

Correlation Between SUV_{max} in Tumor vs. Patient Outcome, PSA, and Immunohistochemistry

Parameter compared with SUV _{max}	Correlation
Time from imaging injection to death	Pearson $r = -0.12$, $P = 0.62$ ($n = 19$)
Time on DSTP3086S ADC treatment	Pearson $r = -0.59$, $P = 0.054$ ($n = 16$)
Baseline PSA level	Pearson $r = 0.1$, $P = 0.67$ ($n = 19$)
Maximal PSA change after DSTP3086S ADC treatment vs. baseline	Pearson $r = -0.496$, $P = 0.576$ ($n = 16$)
Highest immunohistochemistry value (archival or fresh) vs. SUV _{max}	Spearman $r = 0.37$, $P = 0.12$ ($n = 19$)
Immunohistochemistry value for fresh tissue vs. SUV _{max}	Spearman $r = 0.0976$, $P = 0.803$ ($n = 6$)

positive for metastatic prostate cancer with the exception of 1 negative bone biopsy, which on review of the CT-guided interventional biopsy images was attributed to the biopsy's being performed on tissue immediately superior to the ⁸⁹Zr-DFO-MSTP2109A site. This site was strongly suspected to be metastatic because it was also positive on both ¹⁸F-FDG imaging and ⁸⁹Zr-anti-PSMA antibody scanning (data not shown) (20), and a repeat biopsy of this site 220 d after ⁸⁹Zr-DFO-MSTP2109A confirmed metastatic disease. The uptake of ⁸⁹Zr-DFO-MSTP2109A in the 12 contemporaneously biopsied sites in bone showed high uptake, with a median SUV_{max} of 10.7 (range, 3.0–24.8; Supplemental Table 1), except for 2 biopsied tumor sites that had a low SUV, including an expansive rib lesion in patient 1 with an SUV_{max} of 3.2 and a left iliac bone lesion (patient 9; SUV, 3.0). Four biopsied nodal sites in soft tissue had a median SUV_{max} of 11.9 (range, 6.0–17.0). Other nonbiopsied soft-tissue sites that were also positive on antibody imaging and not identified on CT included nodes (usually small or in an atypical location such as supraclavicular or axillary), lung, liver, and prostatic bed.

Bayesian Analysis

We applied Bayesian analysis to data obtained from bone biopsies to estimate the probability that a ⁸⁹Zr-DFO-MSTP2109A-positive bone lesion is biopsy-positive. There were 12 biopsies, 11 of which were positive for ⁸⁹Zr-DFO-MSTP2109A, which leads to a Bayesian estimate of 0.86 for the probability that a ⁸⁹Zr-DFO-MSTP2109A-positive bone lesion is biopsy-positive. The 90% Bayesian confidence interval for this estimate is 0.73–0.99. Supplemental Figure 2 demonstrates the probability density with our estimates marked.

Safety

A safety assessment was performed by serial measurement of blood pressure, heart rate, and temperature. No significant differences were observed for any of these parameters from baseline (1-way ANOVA, $P = 0.067$ – 0.98). Four patients had adverse events. Two patients had grade 1 chills felt to be related to the antibody infusion on the day of injection, one of whom was treated with diphenhydramine. One patient had nausea and vomiting, and another had back

pain, neither of which was believed to be related to the study drug. Serious adverse events were noted in 2 patients: one of these events occurred before antibody infusion, and the other was sepsis due to a urinary tract infection that was considered unrelated to the study drug.

DISCUSSION

Overall, ⁸⁹Zr-DFO-MSTP2109A was well tolerated, with very minor side effects attributable to the injected antibody and consistent with those observed for other antibodies, such as low-grade fever or chills.

A prerequisite to using any antibody as an imaging agent is demonstrating its ability to localize in sites of disease. Preliminary preclinical studies showed good localization of ⁸⁹Zr-DFO-MSTP2109A in prostate xenografts (14). This study confirmed preclinical work and showed localization of ⁸⁹Zr-DFO-MSTP2109A in tumor sites in all patients, extending the imaging findings from our preliminary report on 6 patients that focused on biodistribution, pharmacokinetics, and dosimetry. High-contrast localization was noted in both bone and soft-tissue images in almost all patients when disease was present. This high uptake in bone (median SUV_{max}, 20.6; SUV_{max}, 59.3) compares favorably with that reported for ⁸⁹Zr-DFO-huJ591 anti-PSMA in prostate cancer (mean SUV_{max}, 8.9) or an ⁸⁹Zr-IAB2M anti-PSMA minibody (mean SUV_{max}, 13.8) (20,21). The median SUV_{max} in soft tissue was 16.8, and the maximum SUV_{max} was 24.0, which also compare favorably with the above-referenced antibodies, which showed a mean SUV_{max} of 4.8 and 7 for ⁸⁹Zr-DFO-huJ591 and ⁸⁹Zr-IAB2M, respectively. An additional benefit over these anti-PSMA antibodies is that there is less normal-liver accumulation, which facilitates visualization of liver metastasis.

When conventional imaging modalities or bone scanning only was used as a measure of bone involvement, the sensitivity of ⁸⁹Zr-DFO-MSTP2109A was 62% and 67%, respectively. The positive predictive value of ⁸⁹Zr-DFO-MSTP2109A in bone was 84%, versus 86% for conventional imaging modalities. In addition, 64% of bone sites identified only on ⁸⁹Zr-DFO-MSTP2109A probably corresponded to true sites identified on long-term follow-up with conventional imaging modalities. These findings contrast with those we reported previously for ⁸⁹Zr-DFO-huJ591, which exhibited a higher sensitivity for tumor detection in bone than that we observed here. The reason for the discrepancy in these findings is not clear and may in part be related to differences in study populations or possibly may indicate a difference in biologic expression of STEAP1 versus PSMA in mCRPC. Furthermore, the limitations of bone scans in identifying sites of viable bone disease versus treated nonviable disease are well recognized, as is the identification of false-positive sites. Additional limitations of this study are that it had a small number of patients and confirmation of all image-positive sites was not feasible for ethical reasons; thus, a gold standard for disease was not optimal. Despite these caveats, a large number of metastatic sites were identified as suggested not only by imaging but by biopsy correlation in numerous biopsied sites and by Bayesian analysis, suggesting a probability of 0.86 that a ⁸⁹Zr-DFO-MSTP2109A-positive site is biopsy-positive.

The sensitivity for detection of soft-tissue lesions was 82% (Table 3). ⁸⁹Zr-DFO-MSTP2109A identified an additional 29 soft-tissue lesions not detected on CT, whereas CT identified only 2 additional soft-tissue lesions not detected on ⁸⁹Zr-DFO-MSTP2109A. With long-term follow-up, 41% of the 29 soft-tissue sites identified only on ⁸⁹Zr-DFO-MSTP2109A were identified as abnormal, including 3 sites that were

TABLE 3
Imaging Findings by Modality in Bone or Soft-Tissue Lesions (*n* = 19 Patients)

Agent	Bone lesions						Soft-tissue lesions		Total
	Bone scan+	Bone scan-	CT+	CT-	CIM+	CIM-	CT+	CT-	
⁸⁹ Zr-DFO-MSTP2109A+	433	82	253	262*	443	72	9	29	38
⁸⁹ Zr-DFO-MSTP2109A-	217	48	160	105	265	NA	2	NA	
Total	650	130	413	367	708	72	11	29	

*24 sites identified on ⁸⁹Zr-DFO-MSTP2109A were not in CT field of view; 18 bone scan sites were not in CT field of view.
CIM = conventional imaging modality.

confirmed by biopsy. Compared with prior studies on prostate cancer with ⁸⁹Zr-DFO-huJ591, our study showed a much higher sensitivity for detecting soft-tissue tumor sites; furthermore, in contrast to ⁸⁹Zr-DFO-huJ591, more soft-tissue sites were identified than with CT, some of which were confirmed on long-term follow-up (20).

Although we have previously demonstrated with other antibodies that the degree of tumor uptake is related to tumor antigen concentration, in this study we did not establish a correlation of uptake with antigen based on immunohistochemistry; this may be related to limitations in immunohistochemistry or in tumor sampling. Some variability in SUV in normal organs and tumor is expected, depending on the time from injection to imaging, and could affect correlations of uptake with various parameters. Furthermore, the more rapid removal of antibody from the circulation because of tumor accumulation could also interfere with the correlation of SUV_{max} with immunohistochemistry. Nonetheless, we did observe that the presence of more ⁸⁹Zr-DFO-MSTP2109A-positive bone lesions was related to more rapid clearance of ⁸⁹Zr-DFO-MSTP2109A, although 10 mg of antibody was sufficient to result in high-contrast imaging in patients with mCRPC.

The quantitative analysis of SUV did not correlate with treatment outcomes in patients receiving DSTP3086S ADC, including length of survival from treatment, number of treatments, or time on study. Although not statistically significant, there was a trend toward an inverse correlation of SUV_{max} in any tissue and maximal percentage change in PSA with ADC treatment. This lack of statistical significance may have been related to the small number of patients examined, particularly because a significant number of patients (6/15) discontinued ADC treatment because of side effects and overall there were only minor responses to ADC treatment (data not shown). However, these SUVs were used with a mechanistic pharmacokinetic model of DSTP3086A and preclinical studies of MMAE to confirm that efficacious doses of the ADC toxin MMAE were potentially being delivered to many of the high-uptake lesions imaged. A typical tumor SUV of 20 was equivalent to a several hundred nanomolar concentration of antibody being delivered to the tumor at the maximum therapeutic dose of 2.4 mg/kg. Even when allowing for significant deconjugation of MMAE from the ADC in circulation and a relatively rapid washout of free MMAE from the tumor, the tumor-free toxin is likely to have been in a high tens of nanomolar concentration, considerably above the half-maximal inhibitory concentration of around 1 nM in tumor cell lines. This finding suggests that disappointment in the patient's response rate was more likely caused by insufficient potency of MMAE in these patients' tumors (either innate or through resistance) than by limitations of tumor penetration and drug delivery.

To our knowledge, this is the first study to report in detail on the imaging findings of targeting STEAP1, an antigen newly recognized to be overexpressed in prostate cancer. The difference we observed between targeting PSMA with ⁸⁹Zr-DFO-huJ591 and ⁸⁹Zr-DFO-MSTP2109A in patients with prostate cancer may possibly reflect differences related to the biology of STEAP1- versus PSMA-positive prostate cancer. STEAP1 has not been as extensively studied as the PSMA antigen and warrants further investigation. Lack of response to DSTP3086S ADC probably reflects an issue related to the potency of the ADC rather than delivery or presence of the STEAP1 antigen. Nonetheless, because of the excellent targeting of lesions and the novelty of STEAP1 in prostate cancer, we believe that this reagent warrants further evaluation in patients as a potential predictive biomarker for those undergoing new STEAP1-directed therapy or as a means to identify those who may be more amenable to STEAP1-directed treatment. Although in this study we used 185 MBq, which results in a relatively high radiation dose to normal organs, we feel that lower activities such as the 37–74 MBq used in other studies would be adequate for imaging while decreasing radiation dose.

CONCLUSION

⁸⁹Zr-DFO-MSTP2109A is well tolerated and shows localization in mCRPC sites in bone and soft tissue. Given the high SUV in tumor and localization of a large number of lesions, this reagent warrants further exploration as a companion diagnostic in patients undergoing STEAP1-directed therapy.

DISCLOSURE

This research was supported by the Ludwig Center for Cancer Immunotherapy and NCI grant P01 CA33049. The Clinical Grade Production Radiochemistry Core Facility at Memorial Sloan Kettering Cancer Center is funded in part through NIH/NCI Cancer Center support grant P30 CA008748. This study was also supported by Genentech, Inc. (member of the Roche Group), which holds the right to the antibody; Bernard Fine and Simon Williams are Genentech employees and hold stock in Roche. Steven Larson has received commercial research grants from Genentech, and Jorge Carrasquillo, Michael Morris, Neeta Pandit-Taskar, and Daniel Danila have received research support from Genentech. Steven Larson also receives commercial research grants from WILEX AG, Telix Pharmaceuticals Limited, and Regeneron Pharmaceuticals, Inc.; holds ownership interest/equity in Voreyda Theranostics Inc. and Elucida Oncology Inc.; and holds stock in ImaginAb, Inc. He is the inventor and owner of issued patents both currently unlicensed and licensed by Memorial Sloan Kettering to Samus Therapeutics,

Inc., and Elucida Oncology, Inc. He is or has served as a consultant to Cynvec LLC, Eli Lilly & Co., Prescient Therapeutics Limited, Advanced Innovative Partners, LLC, Gerson Lehrman Group, Progenics Pharmaceuticals, Inc., and Janssen Pharmaceuticals, Inc. Jorge Carrasquillo has received funding support from Chugai Pharmaceuticals Co., Gilead, Regeneron Pharmaceuticals, and Algeta ASA and has served as a consultant for Y-mAbs Therapeutics, Inc., and Bayer. Govind Ragupathi has served as a paid consultant and is a shareholder of MabVax Therapeutics Holdings, Inc., and Adjuvance Technologies. Joseph O'Donoghue is or has served as a consultant to WILEX AG, Algeta ASA, and Janssen Pharmaceuticals, Inc. Michael Morris has served as an unpaid consultant to Astellas Pharma, Inc., Bayer AG, and Endocyte, Inc.; has served as a paid consultant to Advanced Accelerator Applications, Blue Earth Diagnostics, Tokai Pharmaceuticals, Inc., and Tolmar Pharmaceuticals, Inc.; and has received institutional research funding for conducting clinical trials from Bayer AG, Sanofi, Endocyte, Inc., Progenics Pharmaceuticals, Inc., and Corcept Therapeutics, Inc. He has also received funds for travel to academic meetings from Endocyte, Inc., and Bayer AG. Daniel Danila has received research support from the U.S. Department of Defense, the American Society of Clinical Oncology, the Prostate Cancer Foundation, Stand Up 2 Cancer, Janssen Research & Development, Astellas, Pfizer, Medivation, Agensys, and CreaTV. He has served as a consultant to Angle LLT, Janssen Research & Development, Astellas, Medivation, Agensys, and ScreenCell. No other potential conflict of interest relevant to this article was reported.

ACKNOWLEDGMENTS

We thank Jason Lewis, PhD, chief of the Radiochemistry and Imaging Sciences Service; Sonia Sequeira, PhD, head of Product Development; Lee McDonald, PhD, head of the Investigational Products Core Facility; and Elisa de Stanchina, PhD, head of the Antitumor Assessment Core Facility for their support in drug development, as well as Amabelle Lindo, RN, and Louise Harris, RN, for nursing support; Bolorsukh Gansukh and Abigail Boswell for research support; Rashid Ghani, PharmD, and the radiopharmacy group for radiopharmacy support; and Leah Bassity, MA, and Garon Scott for editorial expertise.

KEY POINTS

QUESTION: Is the six-transmembrane epithelial antigen of prostate-1 (STEAP1) a good target for imaging metastatic castration-resistant prostate cancer (mCRPC)?

PERTINENT FINDINGS: This is a prospective clinical trial using ^{89}Zr -DFO-MSTP2109A anti-STEAP1 antibody in 17 patients with mCRPC. Excellent localization of the antibody was noted in bone and soft-tissue metastasis with median SUV_{max} of 20.6 and 16.8, respectively. Sixteen of 17 lesions biopsied were positive on ^{89}Zr -DFO-MSTP2109A and all were histologically positive.

IMPLICATIONS FOR PATIENT CARE: ^{89}Zr -DFO-MSTP2109A shows localization in mCRPC sites in bone and soft tissue, demonstrating that STEAP1 is a potentially useful target in mCRPC patients.

REFERENCES

1. Bander NH, Milowsky MI, Nanus DM, Kostakoglu L, Vallabhajosula S, Goldsmith SJ. Phase I trial of ^{177}Tl -labeled J591, a monoclonal antibody to prostate-specific membrane antigen, in patients with androgen-independent prostate cancer. *J Clin Oncol*. 2005;23:4591–4601.
2. Milowsky MI, Nanus DM, Kostakoglu L, Vallabhajosula S, Goldsmith SJ, Bander NH. Phase I trial of yttrium-90-labeled anti-prostate-specific membrane antigen monoclonal antibody J591 for androgen-independent prostate cancer. *J Clin Oncol*. 2004;22:2522–2531.
3. Tagawa ST, Milowsky MI, Morris M, et al. Phase II study of lutetium-177-labeled anti-prostate-specific membrane antigen monoclonal antibody J591 for metastatic castration-resistant prostate cancer. *Clin Cancer Res*. 2013;19:5182–5191.
4. Pandit-Taskar N, O'Donoghue JA, Beylgeril V, et al. Zr-89-huJ591 immuno-PET imaging in patients with advanced metastatic prostate cancer. *Eur J Nucl Med Mol Imaging*. 2014;41:2093–2105.
5. Kratochwil C, Bruchertseifer F, Rathke H, et al. Targeted alpha-therapy of metastatic castration-resistant prostate cancer with Ac-225-PSMA-617: dosimetry estimate and empiric dose finding. *J Nucl Med*. 2017;58:1624–1631.
6. Kratochwil C, Giesel FL, Stefanova M, et al. PSMA-targeted radionuclide therapy of metastatic castration-resistant prostate cancer with Lu-177-labeled PSMA-617. *J Nucl Med*. 2016;57:1170–1176.
7. Afshar-Oromieh A, Holland-Letz T, Giesel FL, et al. Diagnostic performance of Ga-68-PSMA-11 (HBED-CC) PET/CT in patients with recurrent prostate cancer: evaluation in 1007 patients. *Eur J Nucl Med Mol Imaging*. 2017;44:1258–1268.
8. Morris MJ, Eisenberger MA, Pili R, et al. A phase I/IIA study of AGS-PSCA for castration-resistant prostate cancer. *Ann Oncol*. 2012;23:2714–2719.
9. Hubert RS, Vivanco I, Chen E, et al. STEAP: a prostate-specific cell-surface antigen highly expressed in human prostate tumors. *Proc Natl Acad Sci USA*. 1999;96:14523–14528.
10. Moreaux J, Kassambara A, Hose D, Klein B. STEAP1 is overexpressed in cancers: a promising therapeutic target. *Biochem Biophys Res Commun*. 2012;429:148–155.
11. Gomes IM, Maia CJ, Santos CR. STEAP proteins: from structure to applications in cancer therapy. *Mol Cancer Res*. 2012;10:573–587.
12. Ihlaseh-Catalano SM, Drigo SA, de Jesus CMN, et al. STEAP1 protein overexpression is an independent marker for biochemical recurrence in prostate carcinoma. *Histopathology*. 2013;63:678–685.
13. Barroca-Ferreira J, Pais JP, Santos MM, et al. Targeting STEAP1 protein in human cancer: current trends and future challenges. *Curr Cancer Drug Targets*. 2018;18:222–230.
14. Williams SP, Ogasawara A, Tinianow JN, et al. ImmunoPET helps predicting the efficacy of antibody-drug conjugates targeting TENB2 and STEAP1. *Oncotarget*. 2016;7:25103–25112.
15. Doran MG, Watson PA, Cheal SM, et al. Annotating STEAP1 regulation in prostate cancer with ^{89}Zr immuno-PET. *J Nucl Med*. 2014;55:2045–2049.
16. O'Donoghue JA, Danila DC, Pandit-Taskar N, et al. Pharmacokinetics and biodistribution of ^{89}Zr -DFO-MSTP2109A anti-STEAP1 antibody in metastatic castration-resistant prostate cancer patients. *Mol Pharm*. May 22, 2019 [Epub ahead of print].
17. Danila DC, Szmulewitz RZ, Baron AD, et al. A phase I study of DSTP3086S, an antibody-drug conjugate (ADC) targeting STEAP-1, in patients with metastatic castration-resistant prostate cancer (CRPC) [abstract]. *J Clin Oncol*. 2014;15(suppl):5024.
18. Vosjan MJ, Perk LR, Visser GWM, et al. Conjugation and radiolabeling of monoclonal antibodies with zirconium-89 for PET imaging using the bifunctional chelate p-isothiocyanatobenzyl-desferrioxamine. *Nat Protoc*. 2010;5:739–743.
19. Holland JP, Sheh YC, Lewis JS. Standardized methods for the production of high specific-activity zirconium-89. *Nucl Med Biol*. 2009;36:729–739.
20. Pandit-Taskar N, O'Donoghue JA, Durack JC, et al. A phase I/II study for analytic validation of Zr-89-J591 immunoPET as a molecular imaging agent for metastatic prostate cancer. *Clin Cancer Res*. 2015;21:5277–5285.
21. Pandit-Taskar N, O'Donoghue JA, Ruan ST, et al. First-in-human imaging with Zr-89-Df-IAB2M anti-PSMA minibody in patients with metastatic prostate cancer: pharmacokinetics, biodistribution, dosimetry, and lesion uptake. *J Nucl Med*. 2016;57:1858–1864.